Received: 9 December 2019 | Revised: 22 February 2020 | Accepted: 9 April 2020

DOI: 10.1002/mdp2.177

REPORT

WILEY

Transient simulation of failures during start-up and power cut of a solid oxide fuel cell system using multiphysics modeling

Konrad W. Eichhorn Colombo[1] | **Vladislav V. Kharton**[2] | **Filippo Berto**[3] | **Nicola Paltrinieri**[3]

[1]Department of Chemical Engineering, Norwegian University of Science and Technology (NTNU), Trondheim, Norway

[2]Laboratory of Materials for Electrochemical Technologies, Institute of Solid State Physics RAS, Chernogolovka, Russian Federation

[3]Department of Mechanical and Industrial Engineering, NTNU, Trondheim, Norway

Correspondence
Konrad W. Eichhorn Colombo, Department of Chemical Engineering, Norwegian University of Science and Technology (NTNU), Trondheim, Norway.
Email: konrad.eichhorn@ntnu.no

Abstract

We investigate failure incidents of a solid oxide fuel cell (SOFC) system during start-up from ambient conditions as well as during operation around the design point, using numerical simulation with a view to performance and thermo-mechanical stresses. During start-up, which comprises heating and load ramping phases, the system's trajectory moves through a relatively large temperature range. The simulated failure scenarios include reversible operational discontinuities in terms of input parameters and irreversible hardware failures. Furthermore, we also present results for a complete power cut. A multiphysics modeling approach is used to couple thermal, electrochemical, chemical, and thermo-mechanical phenomena by means of time-dependent partial differential, algebraic, and integral equations. Simulations revealed that the system can smooth out thermal discontinuities that are within a few minutes, that is, within the range of its thermal inertia. However, during the initial phase of the start-up procedure, thermo-mechanical stresses are relatively high due to larger differences between the sintering (manufacturing) and operation temperature, which makes the system more susceptible to failure. This work demonstrates that a multiphysics approach with control- and reliability-relevant aspects leads to a realistic problem formulation and analysis for practical applications.

KEYWORDS

energy, failure, industrial applications, lifetime prediction, multiscale models, reliability, stress analysis, thermomechanics

1 | INTRODUCTION

Fuel cells (FCs) represent a crucial building block for green energy solutions for power generation,[1,2] also as part of a larger system network,[3-5] and for transportation.[2,6] Various FC technologies have been developed,[7-13] where solid oxide fuel cells (SOFCs) have certain advantages over other types of FC, such as the potential use of

nonprecious metals. SOFCs have therefore been intensively studied.[13-18] Nevertheless, issues remain to obtain a sufficient lifetime for wide application. Important challenges include irreversible degradation of electrode, electrolyte, and sealing materials.[19-22]

Due to the complexity and mutual interaction of physical phenomena as well as strong dependence on operation conditions, mathematical modeling is indispensable to gain insight about performance for realistic and critical scenarios. In addition to an electrochemical perspective to assess thermodynamic performance,[23,24] a systems perspective should also take into account thermo-mechanical aspects[25,26] to analyze overall metrics that specify the system's lifetime, such as reliability.[27-35]

Operation under relatively benign conditions in terms of transient gradients already leads to complex control strategies, because of the number of physical variables that need to be controlled as well as material and operational constraints. For safe and economically feasible system start-up, further requirements need to be addressed,[36,37] for example, the use of inert gas (so-called safety gas)[38] to maintain proper conditions with respect to chemical potential in the material and thus avoiding excessive stresses under rapid transients. However, compared with studies that are concerned with design point and off-design/part-load performance, relatively few works exist on detailed transient behavior on a system level. Even fewer studies directly investigate the start-up behavior with all the aforementioned physical phenomena despite its critical importance,[39,40] and in particular conducted by the Jülich team.[41-43] In this respect, we consider the multiphysics approach with time-dependent partial differential algebraic integral equations (PDAIEs) as the core element of a more general model-based systems engineering (SE) framework.

A second branch under the umbrella of this framework is reliability analysis. Here, stochastic (statistical and probabilistic) methods are usually employed, for example, to define maintenance requirements,[44-46] which directly links technical system operation with economics. However, the use of multiple terms to cover certain mechanisms for malfunction, the introduction of several fitting parameters, or both, cannot sufficiently capture the complexity of the internal system's physics.

Systems control is another branch within the model-based SE framework, where simplified models in the frequency or time domain are commonly used, for example, based on proportional-integral-derivative controllers[47] or (nonlinear) model predictive control with state estimators.[48,49] To obtain information about a system's transient behavior subject to disturbances (open-loop) step responses are imposed. But the underlying models are in many cases linearized or, in more general terms, reduced order representations of a high-fidelity or simplified physics-based model.

In summary, the model-based SE framework we are using in this work balances the physics, reliability, and control perspective to arrive at a more realistic understanding of failure-induced risks for the SOFC during start-up as well as normal operation compared with a purely thermodynamic performance approach. A broader and more detailed perspective is of critical importance for actual system operation.

To the best of our knowledge, this is the first study that investigates failures of an SOFC during start-up by means of a thermo-mechanical system model in conjunction with practical issues, including the set of degrees of freedom (DOFs) and the need for safety gas.

One separate note is necessary on system shutdown. We assume that for a normal shutdown in absence of an emergency, the inverse of the start-up procedure can be applied, possibly with some adjustments with respect to the durations of individual phases. In the following, we use only start-up but really mean to cover both, start-up and normal shutdown. We also present results for a power cut as part of an emergency shutdown scenario.

2 | SYSTEM DESCRIPTION

2.1 | SOFC-based plant

In this work, one of the most basic SOFC-based plant designs is used, shown in the process flow diagram (PFD) in Figure 1, also with the additional plant equipment that is required for start-up (in blue). Hydrogen is assumed as fuel, which is perhaps the most benign fuel for this and related FC types. More complex fuels would require further auxiliary equipment and add constraints. We generally reckon that some fundamental and pressing issues still need to be resolved for such basic plant designs, which will also be present in more complex designs, such as level of heat integration and operational requirements including fuel.

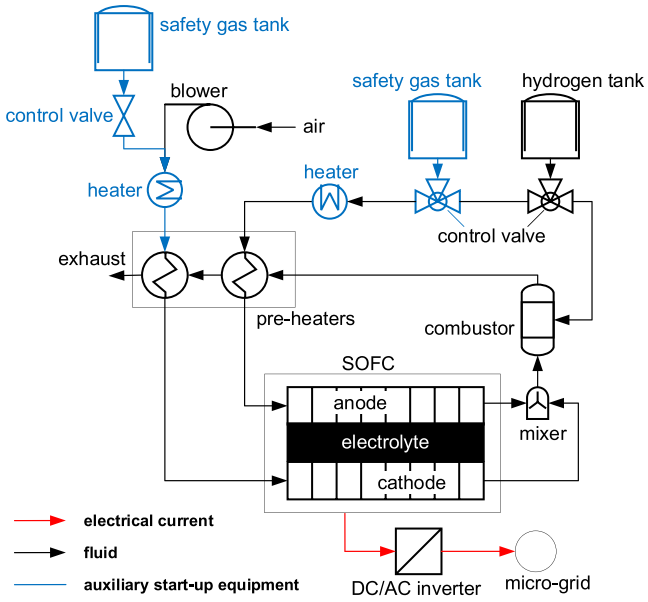

FIGURE 1 Basic solid oxide fuel cell (SOFC)-based system design with auxiliary equipment for start-up/shutdown (in blue)

2.2 | Principal system operation

A simplified FC scheme comprises five components, namely, two gas channels and three ceramic or composite layers. Operation also requires two metallic current collectors (interconnects) and sealants (not shown). The gas channels provide the fluid for reduction (cathode) and oxidation (anode), respectively. Between anode and cathode, there is an oxygen-ion conducting solid electrolyte. Charge neutrality and movement of negative charges (electrons) are provided through an outer electrical circuit. In this work, a tubular design of the SOFC is assumed.[50] The principal mechanism in an individual SOFC is shown in Figure 2.

In the electrochemical cell, oxygen ions are transported from the cathode across the electrolyte membrane to the anode. The half-cell reactions on the cathode (oxygen reduction) and anode (fuel oxidation) are[11]

$$\begin{aligned} O_2 + 4e^- &\rightleftharpoons 2O^{2-}, \\ 2H_2 + 2O^{2-} &\rightleftharpoons 2H_2O + 4e^-. \end{aligned} \tag{1}$$

2.3 | Design and operational constraints

Table 1 summarises critical design and operation constraints of individual process system components of the SOFC-based plant, shown in Figure 1. These determine the overall operation envelope for the SOFC. Even though constraints may be soft, that is, they can be exceeded, doing so may result in major loss of performance, aggregation of irreversibilities, and an associated increase of failure probabilities. The combustor is also critical because it is an active component that provides heat to the system. During start-up of the plant, however, it may be necessary to use a

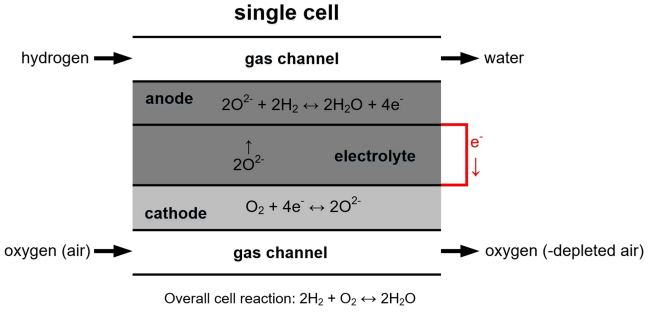

FIGURE 2 Principle of a solid oxide fuel cell (SOFC) with hydrogen as fuel

TABLE 1 Design and operation constraints

Constraint	Potential effect	Limit
Power density	Increasing currents lead to higher concentration polarization and faster cell degradation	80%–90%[51-53]
Max. impurities concentration	Performance loss, degradation, failure	30%[51-53]
Max. leakage rate (interconnects)	Performance loss, failure due to leakage	0.1%[51-53]
Min. temperature	Performance loss, and failure due to thermo-mechanical stresses	900 K[51-53]
Max. temperature	Performance loss and failure due to thermo-mechanical stresses and chemical interaction	1300 K[51-53]
Max. difference in thermal expansion coefficients	Performance loss and failure due to thermo-mechanical stresses	10%–17%[51-53]
Transient temperature gradients	Thermo-mechanical stresses	20K/cm[54,55]
Steady state temperature differences in axial direction of stack	Thermo-mechanical Stresses	150K[51-53]
Min. FU	Thermo-mechanical stresses	40%[51-53]
Max. FU	Fuel starvation, efficiency loss	90%[51-53]
Max. total pressure difference between fluid streams	Mechanical stress	3 bar[51-53]

secondary heat source in conjunction with auxiliary heaters to avoid potential fluctuations and rapid changes due to small thermal inertia.[56] In other words, the short residence time of the fluid may lead to flame instability because of lean operating conditions and high thermal intensity. The preheaters may also add constraints, for example, with respect to total pressure differences across the solid. In this work, we assume that setpoints of all manipulated variables (MVs) can be achieved, no constraints of balance-of-plant system components are therefore considered. Furthermore, purging of gas channels and other preparation tasks for actual system start-up are assumed to be completed.

2.4 | Degrees of freedom

The set of controlled variables (CVs) and MVs for the SOFC system is shown in Table 2. The difference in the number of these two variable types determines the DOF available in the system.[57] Other options for some of the variables are possible. The selection of pairs needs to take into account the measurability of the quantity and the response time. For example, electrical parameters, such as current, will respond faster than those related to heat. In the presence of electrochemically active species at reaction sites (triple-phase-boundaries [TPB]), the SOFC can respond to load variations within the time scale of electrochemistry (within milliseconds).[56]

A physics-based system modeling approach shows a clear benefit regarding the identification of correct CV and MV, because the numerical solution of the model requires a well-posed problem, in other words, an equal number of equations and variables. Input parameters therefore represent the DOF. For example, values of spatially distributed

TABLE 2 Set of controlled and manipulated variables for the SOFC system in Figure 1

Controlled variable	Manipulated variable
Electrical system power	Electrical current
Mean solid temperature of SOFC stack(s)	Blower capacity/mass flow of air
FU of SOFC stack(s)	Fuel valve opening/fuel mass flow to stacks
Pressure gradient across solid of SOFC stack(s)	Use of throttles (not shown in Figure 1)
Combustion outlet temperature	Fuel valve opening/fuel mass flow to combustor
Air temperature to SOFC stack(s)	Bypass ratio of air (not used here)
Chemical kinetics in SOFC stack(s)	Fuel composition (not used here)

Abbreviations: FU, fuel utilization; SOFC, solid oxide fuel cell.

system state variables can usually not (easily) be accessed through direct measurement. Nevertheless, overall system state variables can be defined. A case in point is the mean solid temperature of the SOFC $\bar{T}_s$ (defined below), which is an integral quantity. Such metrics that are based on detailed models provide a better description of system constraints and operation compared with lumped-per-default quantities. The mathematical problem remains well-posed (for numerical solution) irrespective whether MV or CV are specified as input parameters. In this respect, specifying the CV corresponds to the case of perfect control without deviations in measurements of MV, controller actions for CV, or other stochastic effects.

3 | MATHEMATICAL MODEL

In this section, the mathematical model is briefly presented. Further details about the electrochemical model can be found in Stiller et al[58] and Stiller.[59] Notice that a complete description of the thermo-mechanical model, including boundary conditions, is given in our previous work.[50]

3.1 | Energy and mass conservation

Heat, transfer for gas and solid, respectively, read[58-60]

$$\frac{\partial T_g c_{p,g} \rho_g}{\partial t} + v_g \frac{\partial T_g c_{p,g} \rho_g}{\partial z} = \frac{2h_c}{r}(T_s - T_g), \tag{2}$$

$$\rho_s c_{p,s} \frac{\partial T_s}{\partial t} = \lambda_s \nabla^2 T_s. \tag{3}$$

The following boundary condition applies between fuel and the anode, including heat generation through the electrochemical reaction[58,59]

$$\lambda_s \frac{\partial T_s}{\partial r} = h_c(T_s - T_g) + \frac{\dot{r}\Delta h}{2\pi r L}, \tag{4}$$

with the reaction rate[11]

$$\dot{r} = \frac{iA}{2F}. \tag{5}$$

Mass conservation for the gases follows[58-60]

$$\frac{\partial C_i}{\partial t} + v_g \frac{\partial C_i}{\partial z} = \dot{r}_i, \tag{6}$$

3.2 | Electrochemistry

The cell voltage is[11,61]

$$V_{\text{cell}} = V_{\text{OC}} - \eta_{\text{act}}^{\text{an}} - \eta_{\text{act}}^{\text{ca}} - \eta_{\text{con}}^{\text{an}} - \eta_{\text{con}}^{\text{ca}} - \eta_{\text{ohm}}. \tag{7}$$

The open circuit voltage (OCV) is given by the Nernst equation[11,61]:

$$V_{\mathrm{OC}} = E^{\circ} + \frac{\mathrm{RT}}{zF} ln \frac{a_{\mathrm{oxi}}}{a_{\mathrm{red}}}. \tag{8}$$

The activation polarization losses on anode and cathode are given implicitly by the Butler–Volmer equation[11,61]:

$$i_i = i_i^{\circ} \left[\exp\left(\frac{n_i \beta_{fi} F \eta_{\mathrm{act},i}}{\mathrm{RT}} \right) - \exp\left(- \frac{n_i \beta_{ri} F \eta_{\mathrm{act},i}}{\mathrm{RT}} \right) \right]. \tag{9}$$

The concentration polarization losses describe interactions between the bulk gas phase to electrode surfaces as well as between electrode surfaces and TPB[11,61]:

$$\eta_{\mathrm{con},i} = \frac{\mathrm{RT}}{n_i F} \ln(p_{i,\mathrm{g}}, p_{i,\mathrm{TPB}}). \tag{10}$$

The ohmic loss is[11,61]

$$\eta_{\mathrm{ohm}} = i\mathrm{AR}, \tag{11}$$

with an ohmic resistance comprising temperature-dependent resistivity of electrodes and electrolyte and an essentially constant resistivity for the interconnects.[58,59]

3.3 | Thermo-mechanics

The displacement is used as the primary unknown variable. Deformations and displacements of the solid material are relatively small resulting in a system of linear equations.[62] The Navier equations for the electrodes and electrolyte materials in cylindrical coordinates are[63,64]

$$\begin{aligned} \mu\left(\nabla^2 u_r - \frac{u_r}{r^2}\right) + (\lambda+\mu)\frac{\partial}{\partial r}\left(\frac{1}{r}\frac{\partial}{\partial r}(r u_r) + \frac{\partial u_z}{\partial z}\right) &= \beta \frac{\partial \tilde{T}}{\partial r}, \\ \mu \nabla^2 u_z + (\lambda+\mu)\frac{\partial}{\partial z}\left(\frac{1}{r}\frac{\partial}{\partial r}(r u_r) + \frac{\partial u_z}{\partial z}\right) &= \beta \frac{\partial \tilde{T}}{\partial z}. \end{aligned} \tag{12}$$

The displacements are related to the strains according to[64]

$$\begin{aligned} \varepsilon_r &= \frac{\partial u_r}{\partial r}, \\ \varepsilon_\theta &= \frac{u_r}{r}, \\ \varepsilon_z &= \frac{\partial u_z}{\partial z}, \\ \varepsilon_{zr} = \varepsilon_{rz} &= \frac{1}{2}\left(\frac{\partial u_r}{\partial z} + \frac{\partial u_z}{\partial r}\right). \end{aligned} \tag{13}$$

The stress–strain relations are given by Hooke's law[64]

$$\begin{aligned} \sigma_i &= \lambda(\varepsilon_r + \varepsilon_\theta + \varepsilon_z) + 2\mu\varepsilon_i - \beta\tilde{T}, \text{with } i = r,\theta,z, \\ \tau_{zr} &= \tau_{rz} = 2\mu\varepsilon_{zr}. \end{aligned} \tag{14}$$

TABLE 3 Thermo-elastic input parameters

Component	Material	E (GPa)	ν (−)	α (10^{-6}K^{-1})
Anode (reduced)	Ni-3YSZ	$f_2(T)$[27]	0.387[27]	12.6
Electrolyte	8YSZ	$f_3(T)$[27]	0.31[27]	10.9[27]
Cathode	LSM	41[66]	0.28[66]	12[67]

Thermo-mechanical parameters are[63,64]

$$\begin{aligned}\lambda(z) &= \frac{E(z)\nu}{(1+\nu)(1-2\nu)},\\ \mu(z) &= \frac{E(z)}{2(1+\nu)},\\ \beta(z) &= \frac{\alpha E(z)}{1-2\nu}.\end{aligned} \tag{15}$$

The initial stress distribution during the sintering process, with a reference temperature of 1473 K,[65] is assumed to be homogeneously distributed in the material. Further input parameters are given in Table 3. Solving the eigenvalue problem leads to the following algebraic equation system to obtain the principal stresses[68].

$$\begin{aligned}&\sigma_r+\sigma_\theta+\sigma_z=\sigma_1+\sigma_2+\sigma_3,\\ &\frac{1}{2}\left((\sigma_r+\sigma_\theta+\sigma_z)^2-\tau_{rz}^2\right)=\sigma_1\sigma_2+\sigma_2\sigma_3+\sigma_3\sigma_1,\\ &\sigma_r\sigma_\theta\sigma_z-\tau_{rz}^2\sigma_\theta=\sigma_1\sigma_2\sigma_3.\end{aligned} \tag{16}$$

3.4 | System variables

The total current from the SOFC stack is

$$I=\frac{A}{L}\int_0^L i(z)dz, \tag{17}$$

with the DC power

$$P=\mathrm{VI}. \tag{18}$$

Fuel utilization (FU) is an important performance variable and is calculated according to[11]

$$\mathrm{FU}=\frac{I}{2F\dot{n}_{\mathrm{fuel}}}. \tag{19}$$

Overall electrical system efficiency is[69]

$$\eta_{el}=\frac{P}{\dot{n}_{\mathrm{fuel}}\mathrm{LHV}_{\mathrm{fuel}}}. \tag{20}$$

The mean solid temperature is

$$\bar{T}_s = \frac{1}{L}\int_0^L T_s(z)dz. \tag{21}$$

3.5 | Degradation and failure mechanisms

Potential degradation mechanisms for SOFC are complex and often mutually dependent. For example, the actual system design (e.g., tubular or planar) determines to some extent which mechanisms are dominant.[70] The materials being used are other design criteria with a strong effect on performance and duarability.[52] The feedstocks, in particular the fuel and its purity, are further criteria. For instance, the use of carbon-containing fuels, such as natural gas or synthesis gas produced from biomass or coal gasification, can lead to coke formation.[74] Sulfur, even in relatively small amounts, can promote sulfur poisoning.[74-76] Moreover, evaporation of materials from balance-of-plant components may also cause contamination.[77] The complex reaction kinetics are temperature-dependent so that operation conditions strongly affect degradation mechanisms.[78,79]

We assume that the gas supplied to the SOFC is free of any potential contaminants and further employ safety gas to control the electrochemical reactions and chemical potential, respectively. Further uncertainties would be introduced because data are in many cases not available for the entire range of interest for start-up analyses, that is, covering a temperature range from ambient to those required for operation.

The main cause for failure considered in this work are thermo-mechanically induced stresses, with a force-term comprising temperature gradients and differences between the materials with respect to physical properties such as thermal expansion coefficients (Table 3). However, we emphasize that degradation mechanisms may promote or initiate failures, for example, due to material imperfections that are caused during manufacturing or system assembly. These effects are characterized by a high degree of stochasticity.

3.6 | Model implementation and numerical solution

The model was implemented in gPROMS,[80] which is essentially an advanced equation system solver for complex dynamic large-scale problems. In addition to well-posedness, as discussed above, the solvers require a problem formulation of index one. The index determines the smallest number of times the PDAIE must be differentiated to determine continuous functions of the state variables and certain space derivatives of their components.[81,82] The higher the index the more difficult it is to solve the equation system. Individual equations may be reformulated in case models have a too high index for the numerical solvers.[83]

We use finite difference schemes for the discretization of the PDE, with 40 discretization elements in axial direction, 10 discretization elements in radial direction for the cathode, and five for the anode and electrolyte (the cathode is the thickest part of the assembly). The total number of equations is about 19k equations, 18k algebraic, and 1k differential equations. A finer discretization scheme or the use of finite elements methods would have come at the expense of substantially higher computational cost without an associated benefit in terms of principal insights for the SE framework employed in this work. For all simulations, steady state is defined as initial condition. The numerical solution of strongly coupled time-dependent PDAIE system models covering a wide range of values for the state variables, especially in conjunction with discontinuities in time, is relatively demanding for the solvers. We therefore use various techniques to simulate the model from the off-mode at ambient conditions to full load in one continuous run. These techniques include nondimensionalizations and schedules with logical task constructions for initialization values.

Thermodynamic properties are called from the physical property package Multiflash.[80] Thermo-mechanical properties are taken from literature, as shown in Table 3, together with empirical functions for continuous parameter-dependency.

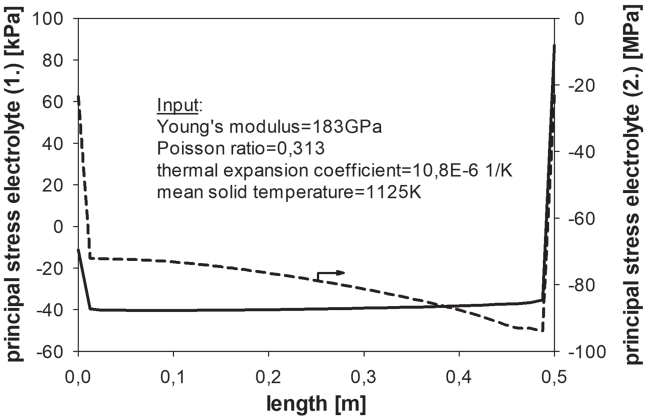

FIGURE 3 Simulation results for validation case

4 | RESULTS AND DISCUSSION

4.1 | Verification and validation

We calculate the overall steady state deviation of energy and mass conservation between the SOFC's inlet and outlets due to the numerical solution, based on

$$\Delta\zeta = 1 - \frac{\sum_k \zeta_{\text{in},k}}{\sum_k \zeta_{\text{out},k}},\ \zeta = \dot{E}, \dot{m}. \tag{22}$$

For the energy balance check, this takes also into account the supplied heat through the feed gas as well as electrochemical reactions. The deviation with respect to energy is about 0.1% and for mass about 0.001%, which is considered as sufficient.

Figure 3 shows the first and second principal stress distributions of the electrolyte. The electrolyte is used for validation because from the three material layers (electrodes and electrolyte), it is where the highest stresses occur and thus most susceptible to failure. The thermo-mechanical properties for Young's modulus, Poisson ratio, and thermal expansion coefficient are for this case taken from Nakajo et al[29] and are also shown in Figure 3, for all following simulations input parameters are as specified in Table 3. Not all required input parameters are given in Nakajo et al[29] and therefore based on our educated guesses (we also use a different length of the SOFC). However, comparison of Figure 3 with Nakajo et al[29*] shows a stress distribution of comparable slope and magnitude.

4.2 | Start-up procedure

The start-up procedure consists of two phases. In the first or heating phase, respectively, the system's temperature is increased by auxiliary heaters, as shown in Figure 4 (see also Figure 1). No electrical power is produced during initial heating. In the second phase, the chemical composition of the two feedgas streams are adjusted, as shown in Figure 5, along with power ramp-up (Figure 4) until the defined design point is reached. In addition to potentially challenging control during the second phase of the start-up procedure, the use of safety gas also represents an additional economic factor. In general, frequent start-up/shutdown cycles should be avoided for economic reasons.

Figures 6 to 8 show the stress distributions in axial direction (z-coordinate) for the electrode-, anode-, and cathode material, respectively (z-coordinate). The profiles correspond to three distinctive times during the start-up of the system: (i) off-mode in which the system is at ambient temperature of 300 K, (ii) power ramp-up where oxygen is supplied to the cathode and hydrogen to the anode, respectively, together with increasing power extraction, and (iii) steady state at the design point. Steady state is reached in less than 15 h. The stresses reduce with the progressing start-up procedure because the force term in the equation set describing thermo-mechanics decreases, or more specifically the difference between sintering temperature (manufacturing) and operation temperature. From the two electrode and the solid

*Bottom of Figure 4.

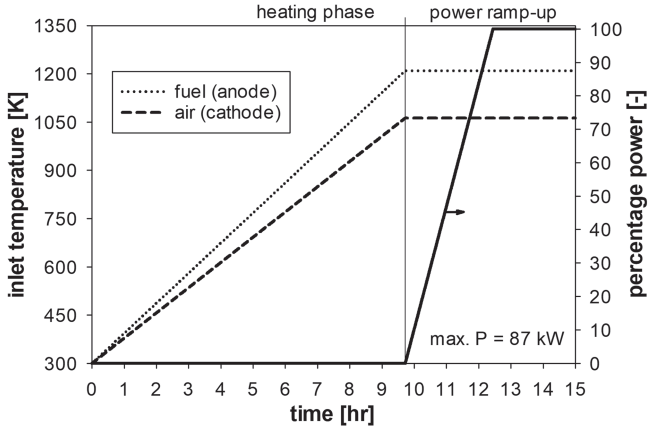

FIGURE 4 Ramping of manipulated variables—fluid temperatures and power

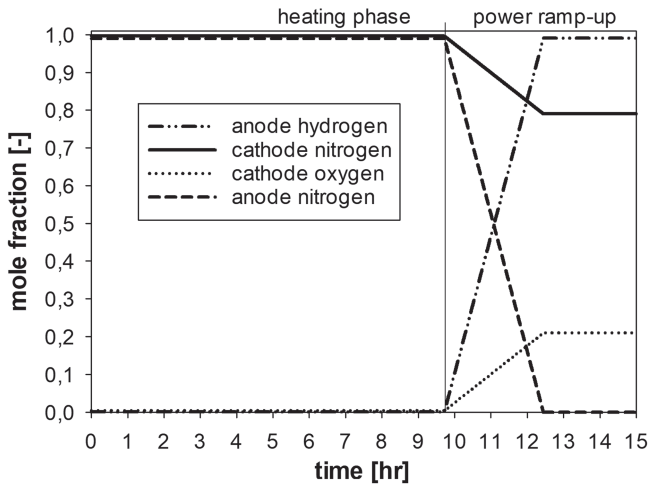

FIGURE 5 Ramping of manipulated variables—fluid compositions

electrolyte materials, the largest stresses occur in the latter one, because the value for Young's modulus is higher compared with those of the electrodes. On the other hand, its thermal expansion coefficient is lower (Table 3) and also directly affects the magnitude of the force terms for thermo-mechanical stresses.

4.3 | Thermodynamic steady state performance

Figure 9 shows the solid temperature and current density in axial direction of the SOFC under normal operation conditions after more than 15 h from initiating the start-up procedure (Figures 4 and 5) without failures. The voltage is 0.55 V. The current density is a function of temperature but also of fuel and oxidant utilization through the electrochemical reactions and therefore varies in axial direction.

4.4 | Irreversible hardware failure during start-up

As an example of a hardware failure is the scenario in which 5% of cells in the stack fail with a corresponding total of 60 cells. An alternative interpretation of this failure incident is the loss of one or more individual modules the SOFC stack is made of. The failure is initiated after 10 h after completion of the heating phase and at the beginning of the power ramp-up phase (Figure 4). The heat distribution in the system remains relatively unaffected by this failure incident in terms of thermo-mechanical stresses, because the thermal inertia are large in comparison with changes in electrical state variables. The effect of this failure incident on FU, which is one of the CVs (Table 2), is shown in Figure 10. The start-up procedures with and without loss of cells are compared. If no controller actions are taken, there will remain an offset in FU. The control strategy must thus be flexible enough to adjust to new setpoints of the controllers. These setpoints need to be within the valid regime of the operation envelope and within the range of constraints, respectively (Table 1). Given the strong interdependence between thermal and electrical phenomena, new

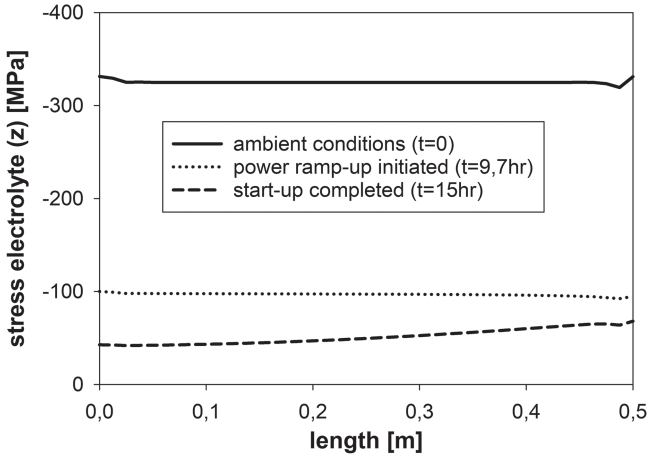

FIGURE 6 Stresses in electrolyte material for *z*-coordinate

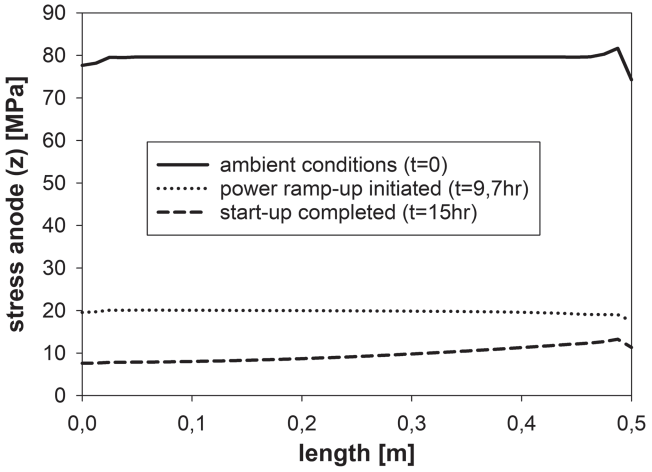

FIGURE 7 Stresses in anode material for *z*-coordinate

setpoints may result in suboptimal performance, operation conditions that favor malfunction, or both. For electrical parameters such as FU, response should be fast because these proceed essentially instantaneously.

4.5 | Reversible discontinuities during operation

During the heating phase, safety gas is fed to the SOFC system (Figure 5), no electrochemical reactions take place and therefore no electrical power is being produced. Technically, the SOFC stack acts as a heat exchanger, in case the temperature of the feedstreams differ from one another. We simulate a reversible failure scenario in which an interruption in the safety gas supply to the anode continues for 5 min, more specifically the molar flowrate drops from 1.15 to 0.15 mol/s. The thermal inertia of the stack are large enough to smooth out this disturbance with respect to heat distribution in the system (numerical results are not shown because of the small effects). Such failure incidents are of practical importance in actual systems and can have different causes, for example, due to the gas tanks in the supply system (Figure 1) or erratic controller behavior. A drop in fuel supply to the anode from 1.1 to 0,95 mol/s for 1 min has again minor effects on the heat distribution (not shown) and thermo-mechanical stress distribution. The system may therefore recover from this incident. However, the FU increases instantaneously to more than 0.91, as shown in Figure 11, which can lead to fuel starvation (Table 1). Fuel starvation may also initiate other irreversible degradation and failure mechanisms. Control systems usually have response times shorter than 1 min, but depending on the variables being monitored such incidents could remain undetected.

4.6 | Power cut

SOFCs are power supply devices, and the customer may demand an immediate power cut from the load. To study the effect of this incident, no changes of the other MVs are imposed (flowrate of air and fuel). The transient system

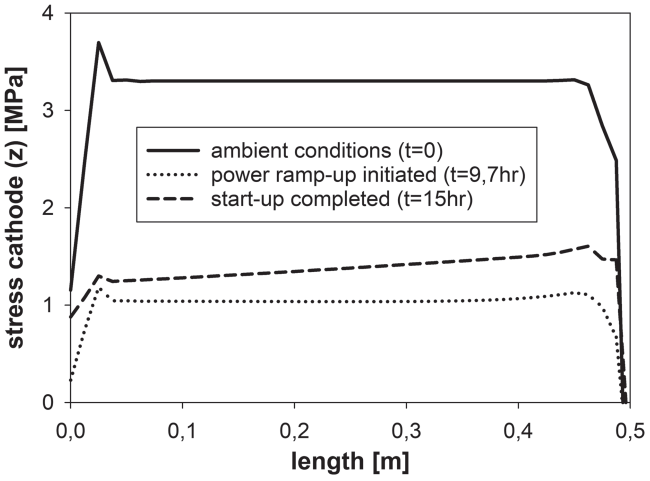

FIGURE 8 Stresses in cathode material for z-coordinate

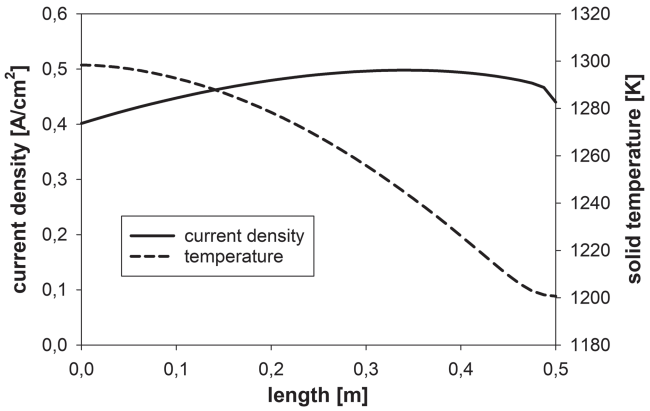

FIGURE 9 Current density and solid temperature under normal operation conditions

response to this incident gives information about the thermal inertia present in the SOFC. Balance-of-plant system components (Figure 1) may add to the overall system thermal inertia. Heat distribution and temperature gradients may therefore be smoothed through forced convection, as long as recycling of fluid or generally supply under these conditions continuous in the system. Here, we consider the case without recycling, which corresponds to the case where all other CVs (Table 2) are kept at the current setpoint. Electrical power enters the energy balance through the electrochemical reaction rate (Section 3.1) so that any changes in power output directly affects the heat distribution in the system. Figure 12 shows the temperature-related constraints from Table 1, that is, the maximum temperature difference in the stack and the maximum temperature gradient. Both remain within the specified limits. The mean solid temperature is also shown in Figure 12. A new steady state after the power cut is reached after about 20 min. Figure 13 shows the displacements in radial and axial direction for the electrodes and electrolyte.

Figure 14 shows that stresses (maximum of absolute) in the materials increase as response to a complete electrical power cut. A new steady state for stress distributions is established based on the heat distribution, as shown in Figure 12.

5 | CONCLUSION

The susceptibility of an SOFC system to operational as well as hardware failure incidents during start-up was investigated, that is, discontinuities in fuel supply, which represents an MV, and a hardware failure in which a certain of cells in the stack fail. Both failures have an effect on the system's operation. While incidents of the former case may be fixed under operation, hardware failures will usually be permanent (replacements disregarded). In case of hardware failures, it is then the extent of expected immediate as well as long-term effects to either continue with the start-up procedure or to abort it. Simulations revealed that the system is able to smooth thermal effects, which occur within a few minutes, in other words which are within the range of thermal inertia. However, during the heating

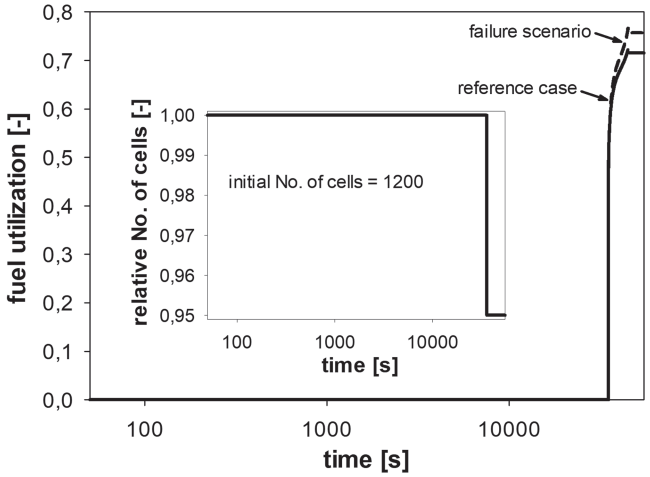

FIGURE 10 Fuel utilization during start-up with and without loss of cells during load increase phase

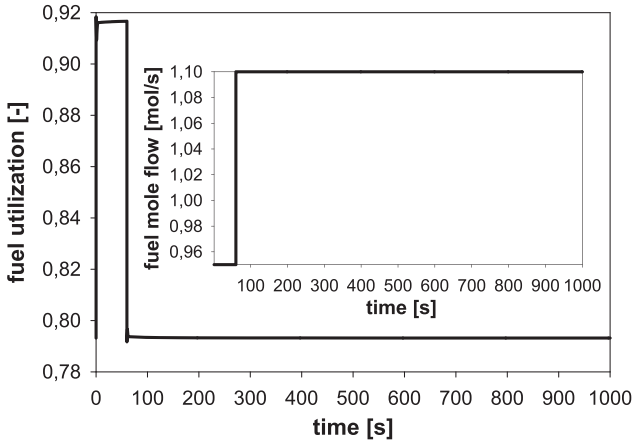

FIGURE 11 Interruption in fuel supply (input disturbance) and fuel utilization (FU) (system's response)

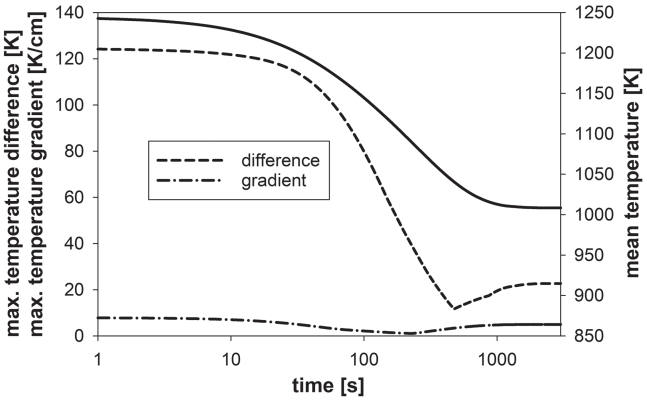

FIGURE 12 Response to power cut of temperature-related quantities specifying constraints

phase, thermo-mechanical stresses are high, and the system is therefore generally more susceptible to failures. In fact, any changes leading to a stronger force term, such as temperature differences between the actual operation and reference temperature (zero stress temperature during manufacturing) will negatively affect the survival probability of the materials. However, elevated sintering temperatures during processing can improve connectivity and ionic conduction. On the other hand, too excessive sintering temperatures may again lead to detrimental effects, primarily due to a decrease in the TPB and specific surface area of the electrodes.[65] Hence, system optimization should consider both, complex dependencies of material properties and operational conditions. Electrical discontinuities have an immediate and strongly detrimental effect on the system's stress distribution. Manipulated system variables as well as critical state variables therefore need to be monitored for a safe start-up procedure in which the system is

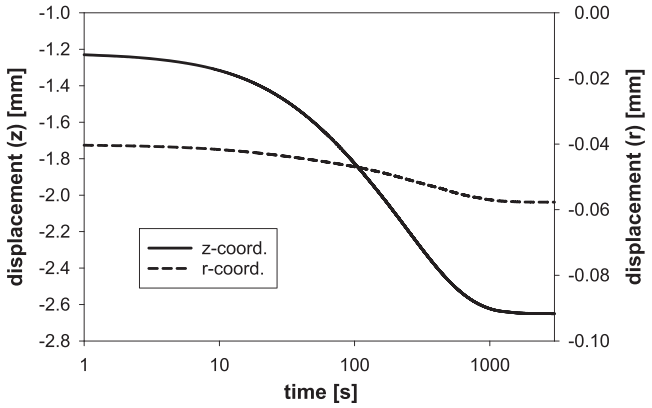

FIGURE 13 Response of system after power cut in terms of displacements

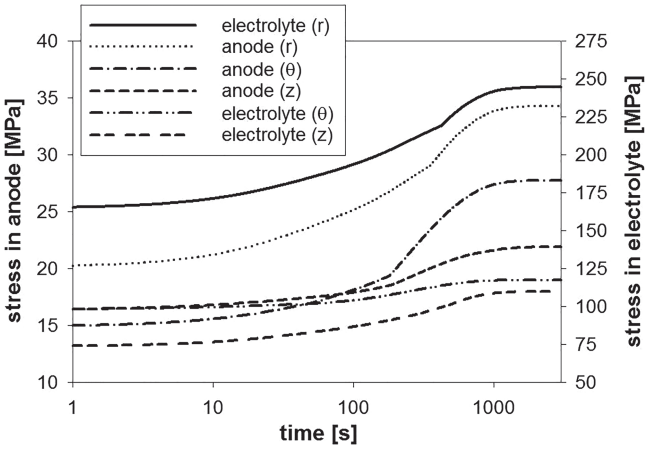

FIGURE 14 Stresses after power cut

exposed to large thermo-mechanical stresses, even in the absence of failures. The number of constraints that need to be respected for safe system start-up as well as interdependence of CVs and MVs in conjunction with elevated stresses lead to relatively strict conditions.

We applied a model-based SE framework in which a combined physics, reliability, and control perspective allowed us to gain a deeper understanding of the system's behavior during start-up under realistic conditions, including potential failure incidents. It was shown that each perspective adds critical insights to make correct assumptions for practical application, such as the identification of material and operational constraints and the available DOFs in the system. For the simulated abrupt electrical power cut, for example, one may be tempted to assume that this incident is not severe for the system in terms of durability when using a thermodynamic model, even when considering temperature-related constraints (as shown in Table 1), while in fact relatively large stresses occur in the materials.

The multiphysics modeling approach with time-dependent PDAIE as core element is well established in the physical science and high-fidelity modeling within SE. But its integration into a bigger framework for reliability analyses, also considering system control, is just at the beginning of being explored and used. Even though electrochemical systems such as SOFC are highly interesting for this methodology due to the number and complexity of physical phenomena that need to be considered, it is applicable to essentially any complex technical system.

ACKNOWLEDGEMENT

Dr Christoph Stiller is gratefully acknowledged for providing the original SOFC model code. The experimental data used to calculate input parameters in this work were collected in the framework of the Russian Science Foundation project 20-19-00478. We thank the anonymous reviewers who made it possible to substantially improve this paper.

SYMBOLS

A area (m^2)
a activity (-), constant for degradation rate (-)

C gas concentration (mol/m^3)
c_p heat capacity [J/(mol K)]
E Young's modulus (Pa), energy (W)
E° Gibbs potential (V)
F Faraday constant (C/mol)
FU fuel utilization (-)
h_c heat transfer coefficient [W/(m^2 K)]
i current density (A/m^2)
L length (m)
LHV lower heating value (J/mol)
$\dot{n}$ mole flow (mol/s)
p partial pressure (Pa)
P power (W)
R universal gas constant [J/(mol K)], ohmic resistance (Ω)
r radius, spatial distribution variable in radial direction (m)
$\dot{r}$ reaction rate (mol/s)
t time (s, h)
u displacement (m)
v fluid velocity (m/s)
V voltage (V)
T temperature (K)
$\bar{T}$ mean temperature (K)
$\tilde{T}$ temperature difference between operation temperature and sintering temperature (K)
z number of electrons exchanged in global reaction (-), spatial distribution variable in axial direction (m)
α thermal expansion coefficient (1/K)
β constant for Butler–Volmer equation (-), thermo-mechanical coefficient (Pa/K)
λ thermal conductivity [W/(K m)], first Lamé coefficient (Pa)
η overpotential (-), efficiency (-)
ρ density (kg/m^3)
ε strain (-)
μ second Lamé coefficient (Pa)
ν Poisson ratio (-)
σ stress (Pa)
τ shear stress (Pa)

SUBSCRIPTS

act activation polarization loss
con concentration polarization loss
g gaseous
i chemical species
ohm ohmic loss
r spatial *r*-direction
s solid material
TPB triple-phase-boundary
z spatial *z*-direction
θ spatial θ-direction

SUPERSCRIPTS

an anode
ca cathode
el electrolyte

ABBREVIATIONS

CV controlled variable
DOF degrees of freedom
FC fuel cell
FU fuel utilization [-]
MV manipulated variable
PDAIE partial differential algebraic integral equation(s)
PFD process flow diagram
SE systems engineering
SOFC solid oxide fuel cell
TPB triple-phase-boundary

ORCID

Konrad W. Eichhorn Colombo https://orcid.org/0000-0003-4010-1730
Filippo Berto https://orcid.org/0000-0001-9676-9970

REFERENCES

1. Chen H, Cong TN, Yang W, Tan C, Li Y, Ding Y. Progress in electrical energy storage system: a critical review. *Prog Nat Sci*. 2009;19(3):291-312.
2. Edwards P, Kuznetsov V, David W, Brandon N. Hydrogen and fuel cells: towards a sustainable energy future. *Energy Policy*. 2008;36(12):4356-4362. Foresight Sustainable Energy Management and the Built Environment Project.
3. Gu W, Wu Z, Bo R, Liu W, Zhou G, Chen W, Wu Z. Modeling, planning and optimal energy management of combined cooling, heating and power microgrid: A review. *Int J Elect Power Energy Syst*. 2014;54:26-37.
4. Hawkes A, Staffell I, Brett D, Brandon N. Fuel cells for micro-combined heat and power generation. *Energy Environ Sci*. 2009;2(7):729-744.
5. Uzunoglu M, Onar O, Alam M. Modeling, control and simulation of a PV/FV/UC based hybrid power generation system for stand-alone applications. *Renew Energy*. 2009;34(3):509-520.
6. Chan C. The state of the art of electric, hybrid, and fuel cell vehicles. *Proc IEEE*. 2007;95(4):704-718.
7. Kreuer K-D. Proton conductivity: materials and applications. *Chem Mater*. 1996;8(3):610-641.
8. Logan B, Hamelers B, Rozendal R, et al. Microbial fuel cells: methodology and technology. *Environ Sci Tech*. 2006;40(17):5181-5192.
9. Mehta V, Cooper J. Review and analysis of PEM fuel cell design and manufacturing. *J Power Sour*. 2003;114(1):32-53.
10. Minh NQ. Ceramic fuel cells. *J Am Ceram Soc*. 1993;76(3):563-588.
11. O'Hayre R, Cha S, Colella W, Prinz FB. *Fuel Cell Fundamentals*. New Jersey: John Wiley & Sons; 2016.
12. Steele B, Heinzel A. Materials for fuel-cell technologies. *Nature*. 2001;414(6861):345-352.
13. Wang C-Y. Fundamental models for fuel cell engineering. *Chem Rev*. 2004;104(10):4727-4766.
14. Choudhury A, Chandra H, Arora A. Application of solid oxide fuel cell technology for power generation—a review. *Renew Sust Energ Rev*. 2013;20:430-442.
15. Singhal S. Advances in solid oxide fuel cell technology. *Solid State Ionics*. 2000;135(1):305-313. Proceedings of the 12th International Conference on Solid State.
16. Stambouli A, Traversa E. Solid oxide fuel cells (SOFCs): a review of an environmentally clean and efficient source of energy. *Renew Sustain Energy Rev*. 2002;6(5):433-455.
17. Yamamoto O. Solid oxide fuel cells: fundamental aspects and prospects. *Electrochimica Acta*. 2000;45(15):2423-2435.
18. Zhang X, Chan S, Li G, Ho H, Li J, Feng Z. A review of integration strategies for solid oxide fuel cells. *J Power Sources*. 2010;195(3):685-702.
19. Adler S. Factors governing oxygen reduction in solid oxide fuel cell cathodes. *Chem Rev*. 2004;104(10):4791-4843.
20. Ettler M, Timmermann H, Malzbender J, Weber A, Menzler N. Durability of ni anodes during reoxidation cycles. *J Power Sources*. 2010;195(17):5452-5467.
21. Jacobson A. Materials for solid oxide fuel cells. *Chem Mater*. 2010;22(3):660-674.
22. Ormerod R. Solid oxide fuel cells. *Chem Soc Rev*. 2003;32(1):17-28.
23. Andersson M, Yuan J, Sunden B. Review on modeling development for multiscale chemical reactions coupled transport phenomena in solid oxide fuel cells. *Appl Energy*. 2010;87(5):1461-1476.
24. Bessler W, Gewies S, Vogler M. *A New Framework for Physically Based Modeling of Solid Oxide Fuel Cells*, Vol. 53; 2007;1782-1800. POLYMER ELEC-TROLYTES Selection of papers from The 10th International Symposium (ISPE-10)15-19 October 2006, Foz do Igua??-PR, Brazil.
25. Peksen M. Numerical thermomechanical modelling of solid oxide fuel cells. *Prog Energy Combust Sci*. 2015;48:1-20.
26. Timurkutluk B, Mat M. A performance prediction tool for solid oxide fuel cells after single redox cycle. *Fuel Cells*. 2015;15(1):71-89.

27. Greco F, Frandsen H, Nakajo A, Madsen MF, Herle JV. Modelling the impact of creep on the probability of failure of a solid oxide fuel cell stack. *J European Ceramic Soc*. 2014;34,(11):2695-2704. Modelling and Simulation meet Innovation in Ceramics Technology.
28. Molla TT, Kwok K, Frandsen HL. Modeling the mechanical integrity of generic solid oxide cell stack designs exposed to long-term operation. *Fuel Cells*. 2019;19(1):96-109.
29. Nakajo A, Stiller C, Harkegard G, Bolland O. Modeling of thermal stresses and probability of survival of tubular SOFC. *J Power Sources*. 2006;158(1):287-294.
30. Nakajo A, Mueller F, Brouwer J, Herle JV, Favrat D. Mechanical reliability and durability of SOFC stacks. Part I : modelling of the effect of operating conditions and design alternatives on the reliability. *Int J Hydrogen Energy*. 2012;37(11):9249-9268.
31. Nakajo A, Mueller F, Brouwer J, herle JV, Favrat D. Mechanical reliability and durability of SOFC stacks. Part II: Modelling of mechanical failures during ageing and cycling. *Int J Hydrogen Energy*. 2012;37(11):9269-9286.
32. Navasa M, Miao X-Y, Frandsen HL. A fully-homogenized multiphysics model for a reversible solid oxide cell stack. *Int J Hydrogen Energy*. 2019;44(41):23330-23347.
33. Peksen M. 3D transient multiphysics modelling of a complete high temperature fuel cell system using coupled cfd and fem. *I J Hydrogen Energy*. 2014;39(10):5137-5147.
34. Pianko-Oprych P, Zinko T, Jaworski Z. Modeling of thermal stresses in a microtubular solid oxide fuel cell stack. *J Power Sources*. 2015; 300:10-23.
35. Serincan MF, Pasaogullari U, Sammes NM. Thermal stresses in an operating micro-tubular solid oxide fuel cell. *J Power Sources*. 2010; 195(15):4905-4914.
36. Chen M-H, Jiang T. The analyses of the start-up process of a planar, anode-supported solid oxide fuel cell using three different start-up procedures. *J Power Sources*. 2012;220:331-341.
37. Zheng K, Kuang Y, Rao Z, Shen S. Numerical study on the effect of bi-polar plate geometry in the SOFC heating-up process. *J Renew Sustain Energy*. 2019;11(1):014301.
38. Halinen M, Thomann O, Kiviaho J. Experimental study of SOFC system heat-up without safety gases. *Int J Hydrogen Energy*. 2014;39(1): 552-561.
39. Choudhary T. Sanjay Computational analysis of IR-SOFC: transient, thermal stress, carbon deposition and flow dependency,. *Int J Hydrogen Energy*. 2016;41(24):10212-10227.
40. Ki J, Kim D. Computational model to predict thermal dynamics of planar solid oxide fuel cell stack during start-up process. *J Power Sources*. 2010;195(10):3186-3200.
41. Al-Masri A, Peksen M, Blum L, Stolten D. A 3D CFD model for predicting the temperature distribution in a full scale APU SOFC short stack under transient operating conditions. *Appl Energy*. 2014;135:539-547.
42. Peksen M, Al-Masri A, Blum L, Stolten D. 3D transient thermomechanical behaviour of a full scale SOFC short stack. *Int J Hyd Energy*. 2013;38(10):4099-4107.
43. Peksen M. Safe heating-up of a full scale SOFC system using 3d multiphysics modelling optimisation. *Int J Hyd Energy*. 2018;43(1): 354-362.
44. Alaswad S, Xiang Y. A review on condition-based maintenance optimization models for stochastically deteriorating system. *Reliab Eng Syst Saf*. 2017;157:54-63.
45. Van Noortwijk J. A survey of the application of gamma processes in maintenance. *Reliab Eng Syst Saf*. 2009;94,(1):2-21. Maintenance Modeling and Application.
46. Si X-S, Wang W, Hu C-H, Zhou D-H. Remaining useful life estimation—a review on the statistical data driven approaches. *Eur J Oper Res*. 2011;213(1):1-14.
47. Skogestad S, Postlethwaite I. *Multivariable Feedback Control*. Chichester: Analysis and Design Wiley; 2005.
48. Morari M, Lee J. Model predictive control: past, present and future. *Comput Chem Eng*. 1999;23(4):667-682.
49. Henson MA. Nonlinear model predictive control: current status and future directions. *Comput Chem Eng*. 1998;23(2):187-202.
50. Eichhorn Colombo K, Kharton V, Berto F, Paltrinieri N. 044514. *J Electrochem Soc*; 167(4).
51. Vielstich W, Lamm A, Gasteiger HA. *Handbook of Fuel Cells*, Vol. 5: Wiley; 2009.
52. Vielstich W, Lamm A, Gasteiger HA. *Handbook of Fuel Cells*, Vol. 6: Wiley; 2009.
53. NETL. Fuel Cell Handbook US Department of Energy; 2004.
54. Kim-Lohsoontorn P, Priyakorn F, Wetwatana U, Laosiripojana N. Modelling of a tubular solid oxide fuel cell with different designs of indirect internal reformer. *J Energy Chem*. 2014;23(2):251-263.
55. Spivey B, Edgar T. Dynamic modeling, simulation, and mimo predictive control of a tubular solid oxide fuel cell. *J Process Control*. 2012; 22(8):1502-1520. Ken Muske Special Issue.
56. Mueller F, Jabbari F, Brouwer J. On the intrinsic transient capability and limitations of solid oxide fuel cell systems. *J Power Sources*. 2009;187(2):452-460.
57. Sharifzadeh M. Integration of process design and control: a review. *Chem Eng Res Design*. 2013;91(12):2515-2549.
58. Stiller C, Thorud B, Bolland O, Kandepu R, Imsland L. Control strategy for a solid oxide fuel cell and gas turbine hybrid system. *J Power Sources*. 2006;158(1):303-315.
59. Stiller C. Design, operation and control modelling of SOFC/GT hybrid systems. *PhD thesis*; 2006.
60. Bird RB, Stewart WE, Lightfoot EN. *Transport Phenomena*. New York: Wiley; 2006.

61. Gellings PJ, Bouwmeester HJ. Handbook of Solid State Electrochemistry CRC; 1997.
62. Allaire G. *Numerical Analysis and Optimization: An Introduction to Mathematical Modelling and Numerical Simulation*. New York: Oxford University Press; 2007.
63. Hetnarski RB, Eslami MR. *Thermal Stresses-Advanced*: Theory and Applications Springer; 2019.
64. Sadd M. *Elasticity, p. iii*. third edition. Boston: Academic Press; 2009.
65. Hildenbrand N, Boukamp BA, Nammensma P, Blank DH. Improved cathode/electrolyte interface of SOFC. *Solid State Ion*. 2011;192(1): 12-15.
66. Giraud S, Canel J. Young's modulus of some SOFCs materials as a function of temperature. *J Euro Ceramic Soc*. 2008;28(1):77-83.
67. Selċuk A, Merere G, Atkinson A. The influence of electrodes on the strength of planar zirconia solid oxide fuel cells. *J Mater Sci*. 2001; 36:1173-1182.
68. Suresh S. *Fatigue of Materials*. Cambridge: Cambridge University Press; 1998.
69. Liso V, Olesen A, Nielsen M, Kar S. Performance comparison between partial oxidation and methane steam reforming processes for solid oxide fuel cell (SOFC) micro combined heat and power (CHP) system. *Energy*. 2011;36(7):4216-4226.
70. Virkar A. A model for solid oxide fuel cell (SOFC) stack degradation. *J Power Sources*. 2007;172(2):713-724.
71. Boldrin P, Ruiz-Trejo E, Mermelstein J, Bermudez Menendez J, Ramlrez Reina T, Brandon N. Strategies for carbon and sulfur tolerant solid oxide fuel cell materials, incorporating lessons from heterogeneous catalysis. *Chem Rev*. 2016;116(22):13633-13684.
72. Haga K, Adachi S, Shiratori Y, Itoh K, Sasaki K. Poisoning of SOFC anodes by various fuel impurities. *Solid State Ion*. 2008;179(27,): 1427-1431. Solid State Ionics 16: Proceedings of the 16th International Conference on Solid State Ionics (SSI-16), Part II.
73. Hagen A, Rasmussen J, Thydén K. *Durability of Solid Oxide Fuel Cells Using Sulfur Containing Fuels*, Vol. 196; 2011;7271-7276. Proceedings of 2010 European Solid Oxide Fuel Cell Forum.
74. Sasaki K, Haga K, Yoshizumi T, et al. Chemical durability of solid oxide fuel cells: influence of impurities on long-term performance. *J Power Sources*. 2011;196(22):9130-9140.
75. Cheng Z, Zha S, Liu M. Influence of cell voltage and current on sulfur poisoning behavior of solid oxide fuel cells. *Journal of Power Sources*. 2007;172(2):688-693.
76. Wang J-H, Liu M. Computational study of sulfurvnickel interactions: A new svni phase diagram. *Electrochem Commun*. 2007;9(9): 2212-2217.
77. Process systems enterprise. The advanced process modelling company.
78. Chudej K, Heidebrecht P, Petzet V, Scherdel S, Schittkowski K, Pesch H, Sundmacher K. Index analysis and numerical solution of a large scale nonlinear pdae system describing the dynamical behaviour of molten carbonate fuel cells. *ZAMM - J Appl Math Mech/ Zeitschrift fur Angewandte Mathematik und Mechanik*. 2005;85(2):132-140.
79. Martinson WS, Barton PI. Distributed models in plantwide dynamic simulators. *AIChE J*. 2001;47(6):1372-1386.
80. Chudej K, Pesch HJ, Sternberg K. Optimal control of load changes for molten carbonate fuel cell systems: a challenge in pde constrained optimization. *SIAM J Appl Math*. 2009;70(2):621-639.
81. Higham NJ. *Accuracy and Stability of Numerical Algorithms*. Second ed. Philadelphia: Soc Indust Appl Math; 2002.
82. Olver P. *Introduction to Partial Differential Equations*: Springer; 2016.
83. Press WH, Teukolsky SA, Vetterling WT, Flannery BP. *Numerical Recipes. The Art of Scientific Computing*. Hong Kong: Cambridge University Press; 2007.

How to cite this article: Eichhorn Colombo KW, Kharton VV, Berto F, Paltrinieri N. Transient simulation of failures during start-up and power cut of a solid oxide fuel cell system using multiphysics modeling. *Mat Design Process Comm*. 2021;3(5):e177. https://doi.org/10.1002/mdp2.177